Interface Recombination in Depleted Heterojunction Photovoltaics based on Colloidal Quantum Dots

*Kyle W. Kemp, Andre J. Labelle, Susanna M. Thon, Alexander H. Ip, Illan J. Kramer, Sjoerd Hoogland, and Edward H. Sargent**

Interface recombination was studied in colloidal quantum dot photovoltaics. Optimization of the TiO_2-PbS interface culminated in the introduction of a thin ZnO buffer layer deposited with atomic layer deposition. Transient photovoltage measurements indicated a nearly two-fold decrease in the recombination rate around 1 sun operating conditions. Improvement to the recombination rate led to a device architecture with superior open circuit voltage (V_{OC}) and photocurrent extraction. Overall a 10% improvement in device efficiency was achieved with Voc enhancements up to 50 mV being realized.

1. Introduction

In recent years significant performance increases have made colloidal quantum dots (CQDs) a very promising material for photovoltaic applications. Certified results of 7.0% power conversion efficiency,[1] η, have been obtained - a significant improvement over the certified η of 5.1% obtained less than 1 year prior.[2] Because these devices employ the same depleted-heterojunction architecture,[3] we can therefore attribute these performance advances to improvements in the CQDs and the films made thereof. Despite these great achievements there is still a need for better understanding of the underlying mechanisms that govern transport and recombination.

As in all photovoltaic technologies, understanding and reducing recombination is one important avenue to improving performance. CIGS[4,5] and organic photovoltaics[6,7] have both benefited from enhanced physical insights to achieve recent performance efficiency (PCE) records. Dye sensitized solar cells have placed significant emphasis on interface recombination at the TiO_2 electrode-dye absorber surface.[8] This has lead to the advancement of characterization techniques such as impedance spectroscopy[9] and photovoltage transient decay[10] for study of photovoltaic systems. Here we pinpoint the spatial location of performance-limiting recombination in CQD solar cells, and take steps to remedy this mechanism. Specifically, we investigate the role of interface recombination in limiting open-circuit voltage (V_{OC}) and we address this issue through improved control over this interface via introduction of a thin ALD layer.

K. W. Kemp, A. J. Labelle, Dr. S. M. Thon, A. H. IP, Dr. I. J. Kramer, Dr. S. Hoogland, Dr. E. H. Sargent
Department of Electrical and Computer Engineering
University of Toronto, 10 King's College Road, Toronto, Ontario, M5S 3G4, Canada
E-mail: ted.sargent@utoronto.ca

DOI: 10.1002/aenm.201201083

2. Results and Discussion

2.1. Interface Recombination

In colloidal quantum dot solar cells, charge carriers may recombine via interface states at the TiO_2 surface. This process may occur one of two ways: 1) Electrons in the CQD conduction band may recombine with holes in the valence band 2) Cross-recombination may occur accross the interface with electrons in the TiO_2 conduction band recombining with holes in the CQD valence band. This cross-recombination pathway is analgous to the widely reported interface loss mechanism in dye sensitized solar cells.[11–13]

Recombination at absorber/window heterojunction interfaces can be understood using a modified Shockley-Read-Hall model.[14] For a negative conduction band offset such as that depicted in **Figure 1**a, with a highly doped window layer ($N_{D,w} > N_{A,a}$), the interfacial recombination rate can be established using:

$$R = \frac{p_{a,z=0} n_{w,z=0}}{S_n^{-1} p_{a,z=0} + S_p^{-1} n_{w,z=0}} \tag{1}$$

where p_a and n_w are the hole and electron concentrations at the interface in the absorber and window materials, respectively. Here S_n and S_p represent the surface recombination velocities for electrons in the window layer and holes in the absorber. The surface recombination velocities are given by:

$$S_{n,p} = v_{th} \sigma_{n,p} N_d \tag{2}$$

where N_D is the interface trap density, $\sigma_{n,p}$ is the carrier capture cross section of the trap for holes and electrons, and v_{th} is the thermal velocity of the material.

For a highly doped n window layer ($n_w >> p_a$) the recombination rate from Equation 1 reduces to:

$$R = S_p p_{a,z=0} \tag{3}$$

Reduction of interface recombination can be achieved through reduction in either the interface carrier densities or surface recombination velocities as indicated in Equation 3. We explored the relative roles of these phenomena via simulation

© 2013 WILEY-VCH Verlag GmbH & Co. KGaA, Weinheim

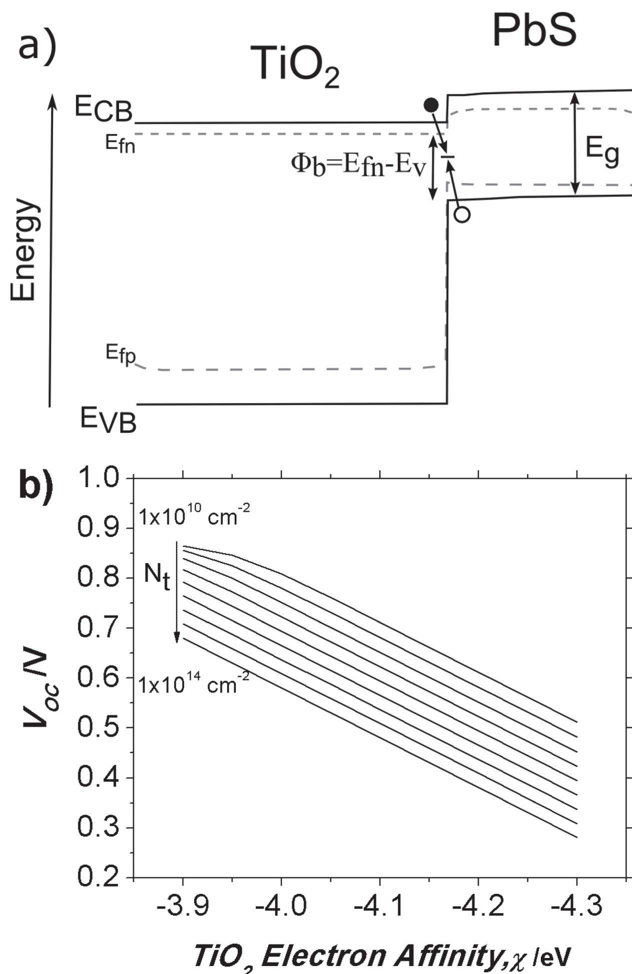

Figure 1. A) Band diagram for PbS-TiO_2 depleted quantum dot heterojunction at open circuit conditions. Interface recombination is depicted as being assisted by interface trap levels. B) Simulation results for V_{OC} as a function of window layer (TiO_2) electron affinity and interface trap density. Trap densities are evenly spaced on a logarthmic scale.

using a SCAPS model[15] developed for the architecture[16,17] in Figure 1a. The parameters employed in the SCAPS model can be found in the supplemental materials.

The absorber hole density at the interface is found to vary with the potential barrier height, Φ_b, according to:

$$p_{a,z=0} = N_v \exp\left(\frac{qV - \phi_b}{kT}\right) \tag{4}$$

Where N_v is the valence band effective density of states, k is the Boltzmann constant, q is the elementary charge, V is the applied voltage and T is the temperature.

From Equation 4 it is apparent that variation in the electron affinity of the window layer (TiO_2) can be used to adjust Φ_b and thus the hole carrier density at the interface. Surface recombination velocities were varied over several orders of magnitude through adjustments in the interface trap density.

2.2. Device Modeling

Simulation results indicate that changing the window layer electron affinity, and also changing the interface trap density, can each have a significant effect on recombination and subsequently V_{OC} (Figure 1b). V_{OC} is predicted to increase 60 mV for every ten fold reduction in interface trap density. A 0.1 eV lowering in the electron affinity of the TiO_2 produced a nearly 0.1 V increase in V_{OC}. In our previous work we examined the effects of TiO_2 electron affinity on performance of quantum dot depleted heterojunctions.[18] While continued work on this path could lead to improved performance, as indicated by simulations, it may be difficult to alter the electron affinity of the window layer without also impacting other properties such as doping density and conductivity.

One unexplored avenue is the modification of the electrode trap state density with the goal of further reducing surface recombination velocities. From Equation 2 this can be achieved either through passivation and removal of interfacial traps or through the reduction in the capture cross section for carriers.

2.3. Interface Modification

Modification of the interface, by introduction of a buffer layer between the TiO_2 and quantum dot film (Figure 1a), may serve to increase performance through reduced recombination and improved V_{OC}. Previous work on dye sensitized solar cells has offered a wide selection of buffer materials to improve the properties of the TiO_2 electrode including Al_2O_3,[19] SiO_2,[20] ZnO,[19] and Nb_2O_5.[19] We decided to investigate these materials as candidate buffer layers in PbS CQD solar cells to reduce interface recombination in our device architecture.

Devices were fabricated based on procedures reported previously.[1] Initial results demonstrated that all buffer materials led to a decrease in device performance (**Figure 2**b) through combined losses in both Fill Factor (FF) and short-circuit current density, J_{SC}. Of particular note is the S-shaped character of the *I–V* curve of the Al_2O_3. This behavior has been observed previously in DSSC[21] and a-Si:H/c-Si[22] solar cells. The Al_2O_3 serves as a tunnel barrier for electron injection from the PbS active layer into the TiO_2. This will lead to an accumulation of minority carriers at the interface resulting in increased recombination and loss to overall carrier collection. No statistical change in V_{OC} was observed for SiO_2, Nb_2O_5, or Al_2O_3. Of the materials studied only ZnO lead to a significant enhancement in V_{OC} indicating its potential as a possible candidate to reduce interface recombination. In order to achieve the necessary improvement in performance optimization of the ZnO layer would be necessary. Addition of ZnO on TiO_2 was found to increase series resistance by approximately 50%, from 6.8 Ω to 10.3 Ω, on average. This is likely a major contributor to the losses in fill factor and J_{SC}.

Optimization of the ZnO buffer layer was carried out to improve fill factor by reducing series resistance. Initial fabrication of ZnO layers from thermal decomposition of zinc acetate required multiple coatings in order to ensure complete coverage of the TiO_2 underneath. A lessening of the series resistance can

© 2013 WILEY-VCH Verlag GmbH & Co. KGaA, Weinheim

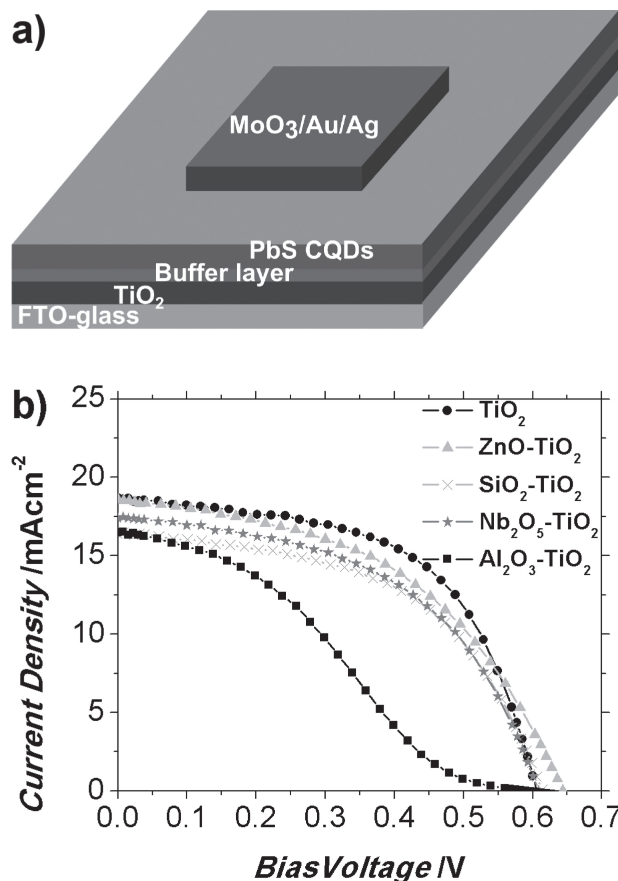

Figure 2. A) Device architecture for CQD depleted heterojunction solar cell with an interfacial buffer layer. B) Device J-V data for modified TiO_2 electrodes with different buffer layer materials.

be achieved by creating, thinner more uniform ZnO layers that completely cover the TiO_2 surface.

With this in mind, we explored the use of atomic layer deposition. Several different thicknesses of ZnO were first attempted and 5 nm was determined to work best. Device data (**Figure 3** a, b, c, d) indicate that the addition of ZnO at the interface led to higher performance through improved Voc and photocurrent collection. A summary of all buffer layers explored in this work can be found in **Table 1**.

Dark *I–V* data was examined to gain further insight into the contributions of the ZnO in this architecture (**Figure 4**). A fit to the linear regime of the forward diode current found that, with the introduction of the ZnO interfacial layer, there was a 100 mV shift in this onset. The improved onset of the dark forward current signifies a reduction in carrier recombination through an improved interface.

To better understand the role of the ZnO, we fabricated ZnO-only-electrode devices employing ALD ZnO on FTO with thicknesses between 5 and 60 nm. The best performing device had a V_{OC} of 0.64, a J_{SC} of 17.5 mA cm^{-2} and a PCE of 3.65%. A series resistance of 15 Ω was obtained and was found to be significantly greater than the resistances for TiO_2 and ZnO-TiO_2 with thicknesses of ~200 nm.[18] This is consistent with the ALD ZnO being highly resistive due to its intrinsic nature. By itself the ALD deposited ZnO does not appear to be suitable for the formation of an efficient heterojunction and only appears to be beneficial as an interfacial buffer layer. In this architecture the underlying TiO_2 is still crucial to form a good N^+p heterojunction with the PbS QD layer.

2.4. V_{OC} Transient Analysis

To better understand how the addition of ZnO leads to improved performance, light-biased V_{OC} transient analysis was performed (**Figure 5**). The ability to do this study with a steady state light bias allows us to characterize the intensity dependence of V_{oc}. There is a clear increase in V_{OC} for the ZnO passivated electrode over the full range of light intensities (Figure 5a).

From the dependence of V_{OC} with intensity it is possible to learn more about the recombination mechanisms limiting performance. Open-circuit voltage varies linearly with the natural logarithm of the photon flux Φ according to:

$$V_{OC} = \frac{nkT\ln(\phi)}{q} + C \tag{5}$$

where n is the ideality factor related to recombination, k is the Boltzmann constant, T is the temperature, q is the elementary charge, and C is a constant. The ideality factor is an indicator of the dominant recombination mechanisms present in an operational solar cell. In the classical SRH model a value of n = 1 represents the ideal case of band-to-band recombination where electrons in the conduction band recombine directly with holes in the valence band. When trap assisted recombination is considered from interface or mid-gap states values of n can theoretically range from 1–2.

Fitting the intensity dependence of V_{OC}, in the high injection regime, yielded n = 1.41 and n = 1.25 for TiO_2 and ZnO-TiO_2 electrodes respectively. Introduction of the ZnO buffer layer thus reduced the ideality factor, bringing it closer to the ideal case for band-to-band recombination. This implies that the ZnO has reduced the role trap assisted recombination through possible removal of interface states.

Transient photovoltage measurements were used to measure the recombination rate as a function of V_{OC}. The methodology was adapted from previous work conducted on polythiophene: Fullerene solar cells.[23] Recombination rate, R, can be calculated using the injected carrier density n and the carrier lifetime, τ:

$$R = \frac{-n}{\tau} \tag{6}$$

Carrier recombination for both ZnO coated TiO_2 and the TiO_2 control were compared (Figure 5b). Recombination rates as a function of V_{OC} show a nearly two-fold reduction after the introduction of the ZnO buffer layer near 1 sun operating conditions. Here we define 1 sun operating conditions to be the point where J_{SC} is equivalent to that those obtained under AM1.5 conditions (~20 $mAcm^{-2}$). This was found to be ~5×10^{17} $cm^{-2}s^{-1}$.

© 2013 WILEY-VCH Verlag GmbH & Co. KGaA, Weinheim

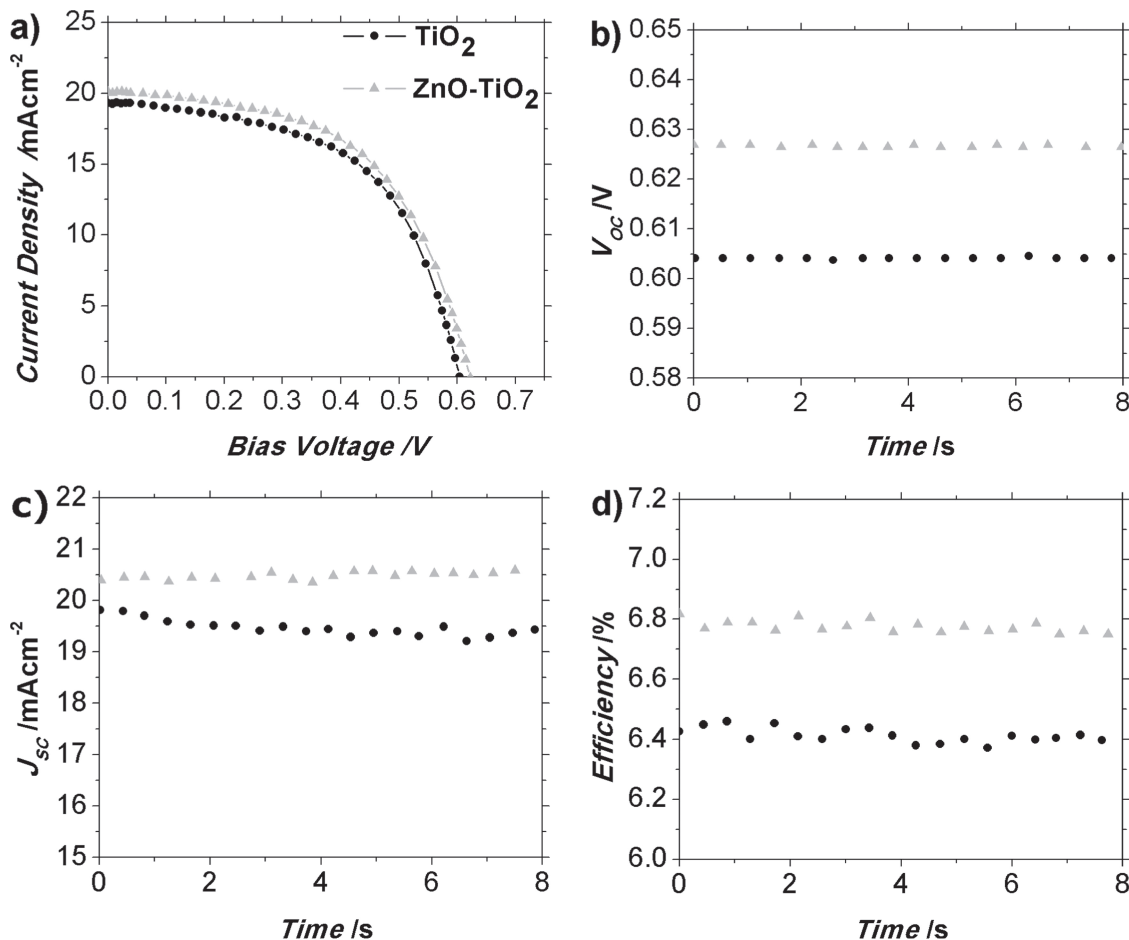

Figure 3. Performance comparison of TiO_2 and modified ZnO-TiO_2 electrodes. A) J-V curves B) Static V_{OC} C) Static J_{SC} D) Static efficiency values at the maximum power point.

The reduction in the recombination rate for the ZnO coated device is due almost entirely to the reduced injection carrier densities (Figure 5c) as opposed to improvements in the carrier lifetimes (Figure 5d). Cyclic voltammetry measurements performed on both TiO_2 and ZnO show that the electron affinity of ZnO is slighly deeper (–4.25 vs –4.15 eV). This would suggest that the addition of ZnO would not lead to an improved Φ_b and that the reduced recombination was instead due to lower surface recombination velocities. This is consistent with the picture of a lower interfacial trap density through passivation and would account for the fact that the recombination rate was achieved through a reduction in $n(V_{OC})$ and not a longer recombination lifetime. In this picture less overall states need to be filled in order to achieve Fermi-level splitting and a higher V_{OC}.

Table 1. Device performance summary for modified TiO_2 electrodes.

Electrode	V_{OC} [V]	J_{SC} [mAcm^{-2}]	FF [%]	Efficiency [%]
TiO_2	0.604 ± 0.004	19.9 ± 0.2	52.8 ± 0.9	6.3 ± 0.1
ZnO-TiO_2 (Initial)	0.65 ± 0.01	17.2 ± 0.9	48.5 ± 0.4	5.1 ± 0.2
SiO_2-TiO_2	0.609 ± 0.008	16.9 ± 0.3	51.9 ± 0.3	5.36 ± 0.05
Nb_2O_5-TiO_2	0.610 ± 0.008	18.0 ± 0.2	50.0 ± 0.4	5.4 ± 0.1
Al_2O_3-TiO_2	0.601 ± 0.006	16.4 ± 0.1	30.8 ± 0.4	2.75 ± 0.04
ZnO-TiO_2 (Optimized)	0.619 ± 0.002	20.7 ± 0.3	54.1 ± 0.6	6.9 ± 0.1

© 2013 WILEY-VCH Verlag GmbH & Co. KGaA, Weinheim

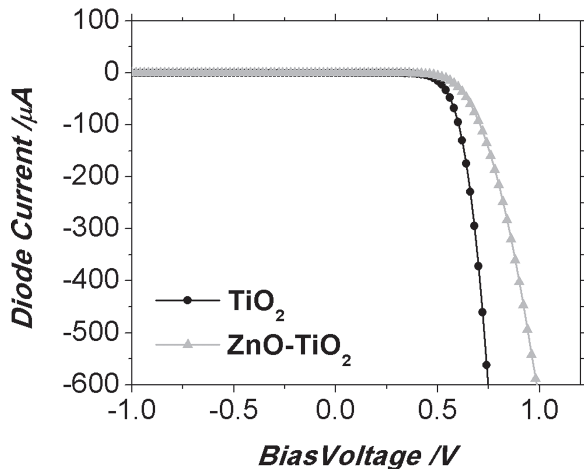

Figure 4. Dark J-V comparison between TiO_2 and ZnO modified TiO_2.

3. Conclusion

Interface recombination was studied in PbS quantum dot photovoltaics. A buffer layer was introduced between TiO_2 and the PbS quantum dots in order to reduce recombination and improve performance. By introduction of a ZnO interfacial layer we were able to improve performance through improved V_{OC} and photocurrent collection. Measurement of recombination rates indicated that the enhanced V_{OC} resulted from a nearly two-fold reduction in carrier recombination at 1 sun conditions.

4. Experimental Section

Electrode Fabrication: TiO_2 substrates were prepared using a Zirconium-doped sol-gel fabrication process used previously.[1,18]

SiO_2 Coating: TiO_2 substrates were placed in an aqueous tetraethyl orthosilicate (Sigma Aldrich) solution (50 mM). The solution was heated in an oven maintained at 90 °C for 30 minutes. Samples were then annealed on a hotplate at 520 °C for 45 minutes.

Nb_2O_5 Coating: A solution (50 mM) of Niobium ethoxide (Sigma Aldrich) in isopropanol (Caledon) was spin cast on TiO_2 substrates at 2500 rpm for 10s at 1000 rpm/s. Substrates were then rinsed with isopropanol and annealed at 520 °C for 45 minutes.

Al_2O_3 Coating: Aluminum oxide was deposited in an atomic layer deposition system from Cambridge Nanotech. Trimethylaluminium (Sigma Aldrich) and H_2O precursors were pulsed sequentially at 0.020 s pulse lengths. This process was repeated 11 times to achieve a thickness of ~1nm. The ALD chamber was maintained at 150 °C throughout the course of the deposition.

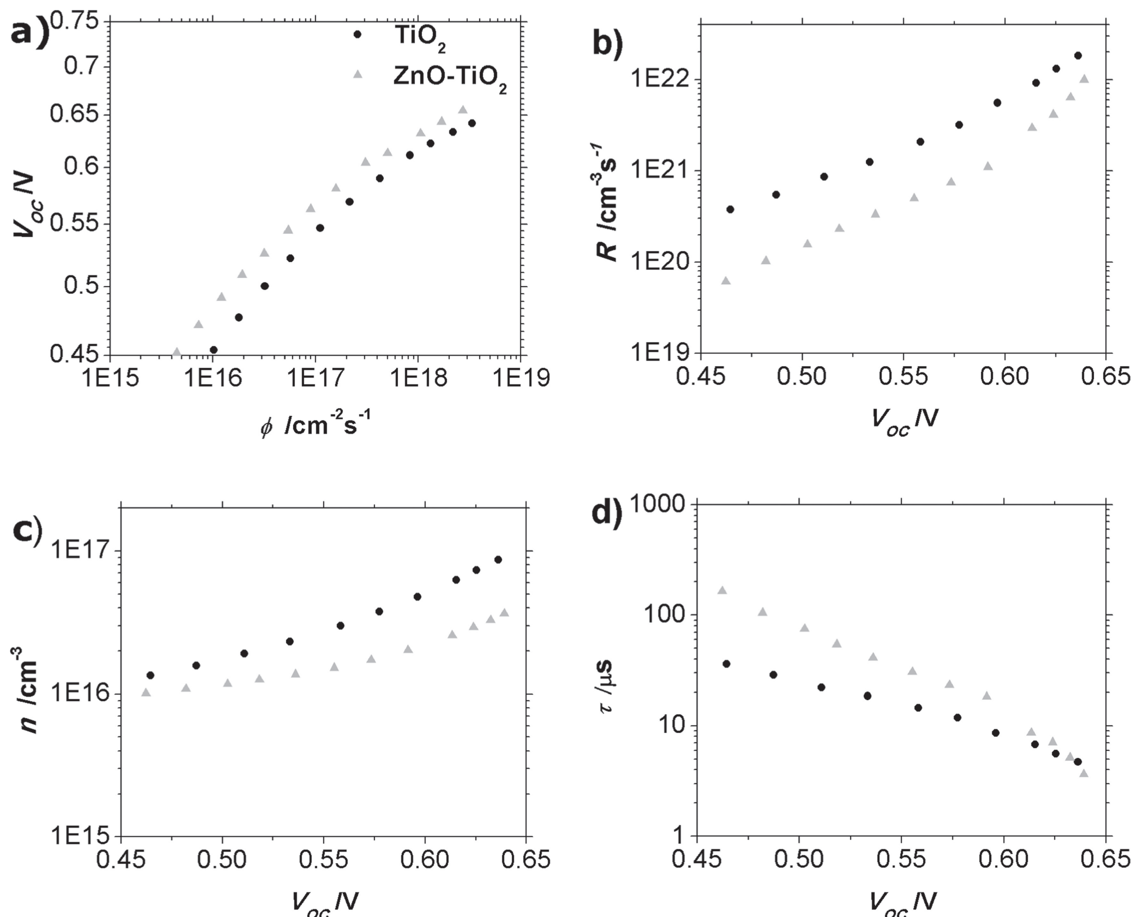

Figure 5. Summary of recombination analysis for TiO_2 and ZnO-TiO_2 substrates. A) V_{OC} as a function of incident photon flux. B) Recombination rates (R) C) Injected carrier densities (n) D) Recombination lifetimes (τ)

© 2013 WILEY-VCH Verlag GmbH & Co. KGaA, Weinheim

ZnO Coating: Initial results on ZnO were obtained through spin casting of Zinc Acetate dihydrate (Sigma Aldrich) in methanol (Caledon) solution (50 mM) on TiO_2 substrates at 1000 RPM and 2.5s acceleration times. Samples were then annealed at 520 °C on a hotplate for 45 minutes. This process was repeated 3 times to ensure complete coverage of the underlying TiO_2.

The optimized ZnO buffer layers were obtained through ALD in a Cambridge Nanotech system. Diethylzinc (Sigma Aldrich) and H_2O precursors were pulsed sequentially at 0.015s pulse lengths. This process was repeated 30 times to achieve a thickness of ~ 5nm. The ALD chamber was maintained at 150 °C throughout the course deposition.

Device Fabrication and Characterization: The PbS CQD film was deposited in a layer-by-layer fashion by spin-casting. PbS CQDs in octane (50 mg/mL) were dispensed on the substrate and spin-cast at 2500 rpm for 10 seconds for each layer. A 3-mercaptopropionic acid:methanol solution (1% v/v)was then dispensed to cover the entire substrate and spun after 3 seconds at the same speed for 5 seconds. Two rinses with methanol were applied for each layer. The top electrode consisting of 15 nm of MoO_3, 50 nm of Au, and 120 nm of Ag was deposited by thermal (MoO_3 and Ag) and electron beam (Au) evaporation at a pressure of $<1 \times 10^{-6}$ Torr. The contact size defined by a shadow-mask was 0.06 cm^2.

V_{OC} Transient Analysis: A modulated 640 nm Melles-Griot diode laser was used to apply a transient V_{OC} signal on top of a steady state light bias from a 830 nm fibre-coupled diode laser. The pulse duration was set to 200 ns with a 50 Hz repetition rate. A neutral density filter was used to control the light intensity reaching the pixel in order to adjust the steady state V_{OC} level. Intensities were varied over the range of 0.0001–5 sun intensities allowing access to a full sweep of V_{OC} levels. The intensity of the 640 nm diode laser was controlled to ensure a constant 10 mV perturbation signal. V_{OC} was measured on an oscilloscope across the 1 MΩ input impedance. The total charge injected from the perturbation pulse was measured from the integration of the laser induced transient signal with the device at J_{SC} conditions.

J–V Characterization: AM 1.5 performance measurements were conducted using a class A (<25% spectral mismatch) solar simulator (ScienceTech). The bias sweep was performed using a Keithley 2400 digital multimeter. The source intensity was measured using a Melles–Griot broadband power meter through a circular aperture of 0.049 cm^2 and set to be 100 mW cm^{-2}. We used an aperture slightly smaller than the top electrode to avoid overestimating the photocurrent: the entire photon fluence passing through the aperture was counted as incident on the device for all analyses of J_{SC} and EQE.[24] The spectral mismatch of the system was characterized using a calibrated reference solar cell (Newport). The total AM1.5 spectral mismatch—taking into account the simulator spectrum and the spectral responsivities of the test cell, reference cell, and broadband power meter—was re-measured periodically and found to be ~11%. This multiplicative factor, M = 0.89, was applied to the current density values of the *J–V* curve to most closely resemble true AM1.5 performance.[25] The test cell was mounted in a thermoelectric-cooled holder with temperature feedback. The testing temperature was measured with a thermal couple and stabilized at 25.0 ± 0.1 °C according to the ISO standard. The total accuracy of the AM1.5 power conversion efficiency measurements was estimated to be ±7%.

Supporting Information

Supporting Information is available from the Wiley Online Library or from the author.

Acknowledgements

This publication is based, in part, on work supported by Award KUS-11-009-21, made by King Abdullah University of Science and Technology (KAUST), by the Ontario Research Fund Research Excellence Program, and by the Natural Sciences and Engineering Research Council (NSERC) of Canada. K.W.K acknowledges support from the Ontario Graduate Scholarship (OGS) program. We thank Angstrom Engineering Inc., Cambridge Nanotech, and Innovative Technology Inc. for useful discussions regarding material deposition methods and control of the glovebox environment, respectively.

Received: December 19, 2012
Revised: February 14, 2013
Published online: March 26, 2013

[1] A. H. Ip, S. M. Thon, S. Hoogland, O. Voznyy, D. Zhitomirsky, R. Debnath, L. Levina, L. R. Rollny, G. H. Carey, A. Fischer, K. W. Kemp, I. J. Kramer, Z. Ning, A. J. Labelle, K. W. Chou, A. Amassian, E. H. Sargent, *Nat. Nano* **2012**, *7*, 577.
[2] J. Tang, K. W. Kemp, S. Hoogland, K. S. Jeong, H. Liu, L. Levina, M. Furukawa, X. Wang, R. Debnath, D. Cha, K. W. Chou, A. Fischer, A. Amassian, J. B. Asbury, E. H. Sargent, *Nat. Mater.* **2011**, *10*, 765.
[3] A. G. Pattantyus-Abraham, I. J. Kramer, A. R. Barkhouse, X. Wang, G. Konstantatos, R. Debnath, L. Levina, I. Raabe, M. K. Nazeeruddin, M. Grätzel, E. H. Sargent, *ACS Nano* **2010**, *4*, 3374.
[4] Clay DeHart. Scharf, C. L. Perkins, B. To, R. Noufi, *Prog. Photovoltaics* **2008**, *16*, 235.
[5] Q. Cao, O. Gunawan, M. Copel, K. B. Reuter, S. J. Chey, V. R. Deline, D. B. Mitzi, *Adv. Energy Mater.* **2011**, *1*, 845.
[6] R. F. Service, *Science* **2011**, *332*, 293.
[7] S. D. Oosterhout, M. M. Wienk, S. S. van Bavel, R. Thiedmann, L. Jan Anton Koster, J. Gilot, J. Loos, V. Schmidt, R. A. J. Janssen, *Nat. Mater.* **2009**, *8*, 818.
[8] Q. Wang, S. Ito, M. Grätzel, F. Fabregat-Santiago, I. Mora-Seró, J. Bisquert, T. Bessho, H. Imai, *J. Phys. Chem. B* **2006**, *110*, 25210.
[9] P. P. Boix, A. Guerrero, L. F. Marchesi, G. Garcia-Belmonte, J. Bisquert, *Adv. Energy Mater.* **2011**, *1*, 1073.
[10] C. G. Shuttle, B. O'Regan, A. M. Ballantyne, J. Nelson, D. D. C. Bradley, J. de Mello, J. R. Durrant, *Appl. Phys. Lett.* **2008**, *92*, 093311.
[11] A. K. Chandiran, N. Tetreault, R. Humphry-Baker, F. Kessler, E. Baranoff, C. Yi, M. K. Nazeeruddin, M. Grätzel, *Nano Lett.* **2012**, *12*, 3941.
[12] J. E. Kroeze, N. Hirata, S. Koops, M. K. Nazeeruddin, L. Schmidt-Mende, M. Grätzel, J. R. Durrant, *J. Am. Chem. Soc.* **2006**, *128*, 16376.
[13] S. Y. Huang, G. Schlichthörl, A. J. Nozik, M. Grätzel, A. J. Frank, *J. Phys. Chem. B* **1997**, *101*, 2576.
[14] R. Scheer, H.-W. Schock, In *Chalcogenide Photovoltaics*; Wiley-VCH, Weinheim **2011**; pp. 9–127.
[15] M. Burgelman, P. Nollet, S. Degrave, *Thin Solid Films* **2000**, *527*, 361–362.
[16] I. J. Kramer, E. H. Sargent, *ACS Nano* **2011**, *5*, 8506.
[17] D. Zhitomirsky, I. J. Kramer, A. J. Labelle, A. Fischer, R. Debnath, J. Pan, O. M. Bakr, E. H. Sargent, *Nano Lett.* **2012**, *12*, 1007.
[18] H. Liu, J. Tang, I. J. Kramer, R. Debnath, G. I. Koleilat, X. Wang, A. Fisher, R. Li, L. Brzozowski, L. Levina, E. H. Sargent, *Adv. Mater.* **2011**, *23*, 3832.
[19] Y. Diamant, S. Chappel, S. G. Chen, O. Melamed, A. Zaban, *Coord. Chem. Rev.* **2004**, *248*, 1271.
[20] H.-J. Son, X. Wang, C. Prasittichai, N. C. Jeong, T. Aaltonen, R. G. Gordon, J. T. Hupp, *J. Am. Chem. Soc.* **2012**, *134*, 9537.
[21] G. Kron, U. Rau, J. H. Werner, *J. Phys. Chem. B* **2003**, *107*, 13258.
[22] X. Bubnova, A. Petersen, F. Einsele, R. Rölver, U. Rau, C. Leendertz, T. Wagner, In *Al_2O_3 as a Passivating and Tunneling Layer for Heterojunction a-Si:H/c-Si Solar Cells*; Frankfurt, Germany; pp. 1538–1543.
[23] R. Hamilton, C. G. Shuttle, B. O'Regan, T. C. Hammant, J. Nelson, J. R. Durrant, *J. Phys. Chem. Lett.* **2010**, *1*, 1432.
[24] B. E. Hardin, H. J. Snaith, M. D. McGehee, *Nat. Photon.* **2012**, *6*, 162.
[25] J. M. Kroon, M. M. Wienk, W. J. H. Verhees, J. C. Hummelen, *Thin Solid Films* **2002**, *223*, 403–404.

© 2013 WILEY-VCH Verlag GmbH & Co. KGaA, Weinheim